Optics Letters

Hidden symmetry-induced effective moving double-zero-index metamaterials

YUHAO JING,[1] ZHONGFEI XIONG,[1] YUNTIAN CHEN,[1,2,3,*] RUO-YANG ZHANG,[4,5] AND C. T. CHAN[4]

[1]School of Optical and Electronic Information, Huazhong University of Science and Technology, Wuhan 430074, China
[2]Wuhan National Laboratory of Optoelectronics, Huazhong University of Science and Technology, Wuhan 430074, China
[3]Optics Valley Laboratory, Wuhan 430074, China
[4]Department of Physics, The Hong Kong University of Science and Technology, Clear Water Bay, Hong Kong SAR, China
[5]ruoyangzhang@ust.hk
*yuntian@hust.edu.cn

Received 13 May 2024; revised 2 June 2024; accepted 16 June 2024; posted 20 June 2024; published 12 July 2024

Materials possessing an effective zero refractive index are often associated with Dirac-like cone dispersion at the center of the Brillouin zone (BZ). It has been reported the presence of hidden symmetry-enforced triply degenerate points [nexus points (NP)] away from the Brillouin zone center with the stacked dielectric photonic crystals. The spin-1 Dirac-like dispersion in the *xy* plane near the nexus point suggests a method for achieving zero refractive index materials. The stacked photonic crystals at the nexus points can be deemed as an effective moving double-zero-index medium (MDZIM) traveling with a speed relative to the laboratory reference. The ability of this moving double-zero-index medium to enable perfect wave tunneling across barriers without reflection has been demonstrated, dependent on the incident waves' specific angular orientations.

https://doi.org/10.1364/OL.529880

Symmetry-protected band degeneracies represent a pivotal topic in topological photonics, facilitating the occurrence of relativistic quasiparticles, such as 3D Weyl and Dirac fermions, within artificial structures [1–5]. Achieving higher-order degeneracies usually hinges on distinct symmetries or intricate space groups. Non-symmorphic symmetries, including glide and screw operations, have facilitated the creation of Kramers-like degeneracies at the boundaries of the first Brillouin zone (BZ), alongside unusual band connections [6]. Traditionally, these degeneracies were thought to be fully captured by the spinless space groups of photonic crystals (PhCs). However, recent advancements have upended this notion, revealing that band topology can be influenced by intrinsic properties of Maxwell's equations not immediately discernible from the space group of material, leading to distinctive photonic band crossings and connectivities [7]. Our previous research [8] has uncovered a hidden geometric symmetry of layer-stacked anisotropic PhCs stemming from the unique form of Maxwell's equations. This hidden symmetry can protect nodal lines to steadfastly intersect at triply degenerate nexus points (NPs). The bands with a constant k_z near the NPs disperse as a spin-1 Dirac-like cone in the xy plane, giving rise to exotic transport features of light and recalling the scheme of realizing a double-zero-index medium (DZIM) with the accidental Dirac-like dispersion at the Γ point in 2D PhCs [9].

Zero-index media (ZIM), distinguished by the disappearance of one or more constitutive parameters, have attracted significant interest over the past decade due to their remarkable properties in wave manipulation [10–12], including directive emission [13,14], wave tunneling [15–17], and wavefront engineering [18,19], while the mismatch between the effective impedance of ZIM and that of general materials is notable. A simply connected 2D DZIM can address this challenge, efficiently coupling with normally incident plane waves [20–23]. An electromagnetic wave with transverse-electric (TE) polarization can traverse a DZIM-filled waveguide without distortion [24], even in the presence of embedded perfect electric conductor (PEC) impurities. In contrast, perfect reflection occurs when the inclusion becomes a perfect magnetic conductor (PMC) object. Despite the compelling attributes of the 2D DZIM, they do not naturally exist. It is established that Dirac-like dispersion can replicate a DZIM system [9], necessitating a spin-1 cone at $\mathbf{k} = 0$, constructed by the accidental triply degenerate band at Γ. Such accidental degeneracy arises from precise material parameter adjustments and is susceptible to perturbations.

In this Letter, we present a novel approach for implementing the moving double-zero-index medium (MDZIM) at $\mathbf{k} = \mathbf{k}^{NP\pm}$ away from the Brillouin zone center with layer-stacked anisotropic PhCs. The center of iso-frequency surfaces of a moving medium will shift along the moving direction due to the Fresnel–Fizeau drag effect [25]. Therefore, the stacked PhC with a shifted Dirac-like cone dispersion behaves as a MDZIM with a z-directed velocity $\mathbf{v} = c^2\mathbf{k}^{NP\pm}/\omega^{NP}$ for quasi-2D waves with a constant $k_z = k_z^{NP\pm}$ at the NPs' frequency. Compared with the 2D DZIM approach based on a fine-tuned triple degeneracy, the symmetry-enforced nature of the triple NPs ensures that an effective MDZIM can be achieved for all PhCs that adhere to the requisite symmetries without

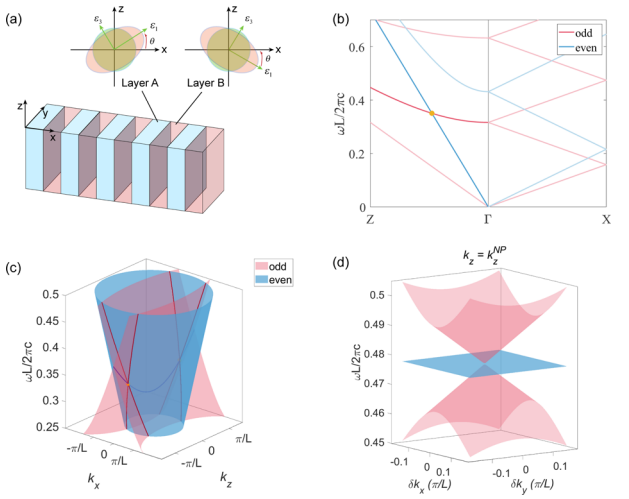

Fig. 1. Layer-stacked photonic crystal made of a generic anisotropic dielectric. (a) Structure of the PhC, where the two insets display the refractive index ellipsoid in the xz plane of the anisotropic dielectrics in different layers. (b) Band structure along high-symmetry lines in the $k_y = 0$ plane for PhC with $\varepsilon_1 = \varepsilon_2 = 10$, $\varepsilon_3 = 1$, and rotation angle $\theta = 2\pi/5$. The lattice constant L is 0.5 μm. The blue and red lines represent the band with odd and even M_y-parities, respectively. The orange dot denotes the threefold degenerate nexus point we concertinaed. (c) 3D band structure of the PhC on the high-symmetry plane $k_y = 0$. A pair of orange dots shows the nexus points of the three nodal lines (two of them for red and another one for blue.) (d) Dirac-like cone band structure at $k_z = k_z^{NP}$ plane.

the need for parameter fine-tuning. We demonstrate that the perfect tunneling effect persists for MDZIMs at specific incident angles, through simulated results of both layer-stacked PhCs and an ideal MDZIM. Additionally, we also include a discussion on universal impedance matching and angle-dependent transmittance, highlighting the parallel properties between PhCs and the ideal MDZIM in terms of tunneling capabilities.

The PhC under investigation is structured from the two types of anisotropic dielectric layers, arranged in a periodic fashion along the x axis while maintaining homogeneity in the transverse yz plane. Each layer shares the same thickness and is crafted from identical nondispersive anisotropic dielectric materials, characterized by principal relative permittivity values of ε_1, ε_2, and ε_3, whereas the optical axes rotate alternatively in different layers, as shown in Fig. 1(a). Specifically, the second principal axis of the materials is fixed along the y direction, while the first principal axis is rotated by an angle θ or $-\theta$ in different layers. Consequently, the relative permittivity tensor of the PhC can be described as follows:

$$\varepsilon_r = \begin{pmatrix} \varepsilon_{xx} & 0 & \varepsilon_{xz} \\ 0 & \varepsilon_{yy} & 0 \\ \varepsilon_{xz} & 0 & \varepsilon_{zz} \end{pmatrix}, \tag{1}$$

where $\varepsilon_{xz} = \varepsilon_{zx} = \pm(\varepsilon_1 - \varepsilon_3 \sin\theta\cos\theta)$ flips its sign between different layers, while the diagonal elements $\varepsilon_{xx} = \varepsilon_1 \cos^2\theta + \varepsilon_3 \sin^2\theta$, $\varepsilon_{yy} = \varepsilon_2$, and $\varepsilon_{zz} = \varepsilon_1 \sin^2\theta + \varepsilon_3 \cos^2\theta$ are all constant. The space group of the layer-stacked PhC is the semidirect product of a 2D continuous translational group $\mathbb{R}^2$ and the 22ed rod group: $\mathbb{R}^2 \rtimes Rod\,(22)$. Thanks to the mirror symmetry M_y in the y direction, the eigenstates in the $k_y = 0$ plane can be sorted by their even or odd M_y-parity. The eigen-frequencies of the M_y-odd and even states have the following analytical expressions:

$$\hat{M}_y - odd : \left(\omega_m^{odd}\right)^2 / c^2 = \frac{1}{\varepsilon_{yy}} \left[\left(k_x + m\frac{2\pi}{L} \right)^2 + k_z^2 \right],$$

$$\hat{M}_y - even : \left(\omega_m^{even}\right)^2 / c^2 = \frac{\varepsilon_{xx}}{\varepsilon_1 \varepsilon_3} \left(k_x + m\frac{2\pi}{L} \right)^2 + \frac{1}{\varepsilon_{xx}} k_z^2,$$

with $m \in \mathbb{Z}$ numbering the bands, L denoting the lattice constant, and c being the light speed in vacuum. The band structure along the high-symmetry lines of the PhC is plotted in Fig. 1(b).

In general, the stationary Maxwell's equations can be written as a generalized eigenvalue problem:

$$\begin{pmatrix} 0 & i\nabla\times \\ -i\nabla\times & 0 \end{pmatrix} \begin{pmatrix} \mathbf{E} \\ \mathbf{H} \end{pmatrix} = \omega \begin{pmatrix} \varepsilon & \chi \\ \chi^\dagger & \mu \end{pmatrix} \begin{pmatrix} \mathbf{E} \\ \mathbf{H} \end{pmatrix}, \tag{2}$$

where we denote the curl matrix and the constitutive matrix on the left and right sides of Eq. (2) as $\hat{N}(\mathbf{r})$ and $\hat{M}(\mathbf{r})$, respectively. The space group symmetries are entirely encoded in the space-dependent constitutive tensor as $\hat{A}\hat{M}(\mathbf{r})\hat{A}^{-1} = \hat{M}(\mathbf{r})$. However, when considering a generic symmetry $\hat{B}$ of Maxwell's equations, it is sufficient to require that the entire effective Hamiltonian remains invariant under $\hat{B}$, expressed as $\hat{B}\hat{H}(\mathbf{r})\hat{B}^{-1} = \hat{H}(\mathbf{r}) = \hat{M}(\mathbf{r})^{-1}\hat{N}$, but allowing for $\hat{B}\hat{M}(\mathbf{r})\hat{B}^{-1} \neq \hat{M}(\mathbf{r})$. This general requirement imposes less stringent constraints than spatial symmetries, suggesting the potential existence of hidden symmetries that transcends standard space groups. In the specific PhC model we analyzed, this nuanced understanding of symmetry enabled the discovery of a generalized 1/4-period screw rotation symmetry, as reported in our earlier work [8]. This hidden symmetry arises from the fractional periodicity characteristic of the dielectric components of Eq. (1) within the PhC, resulting in Kramers-like nodal lines (NLs), each formed by the intersection of two bands with the same M_y parity, along the k_z axis passing through the Brillouin zone (BZ) center, as shown by the two-fold lines along Γ-Z in Fig. 1(b). As shown in Fig. 1(c), the two M_y-odd bands forming the lowest Kramers-like NL (blue) also intersect with the lowest M_y-even band along two mirror-protected NLs (red). These three NLs converge a pair of triple NPs with Bloch wave vectors $\mathbf{k}^{NP\pm} = \left(0, 0, \pm 2\pi/L\sqrt{\varepsilon_{xx}/(\varepsilon_{yy} - \varepsilon_{xx})}\right)$ and angular frequency $\omega^{NP} = 2\pi c/\left(L\sqrt{\varepsilon_{yy} - \varepsilon_{xx}}\right)$. Figure 1(d) illustrates the Dirac-like dispersion in the xy plane near the NPs (see Supplement 1 S1 for more details), which recalls the scheme of realizing the double-zero-index medium (DZIM) with the accidental Dirac-like cone at the Γ point in 2D PhCs [9,26]. This dispersion pattern features two conical branches that reduce to the $\hat{M}_y$-odd bands of the orders $m = \pm 1$ along the line of $k_y = 0$. The flatband reduces to the M_y-even band of $m = 0$ along the line of $k_y = 0$.

We retrieve the effective parameters at NPs by matching the dispersion between the analytical solution obtained from PhC calculations and that from an ideal MDZIM (see Supplement 1 S2 for more details). In the present scenario, the NPs are located away from the Γ point along the k_z direction. While the center of iso-frequency surfaces of a moving medium will shift along the moving direction due to the Fresnel–Fizeau drag effect [25]. Therefore, we expect that the NPs here will shift back to Γ and behave as a DZIM when observed in a moving reference

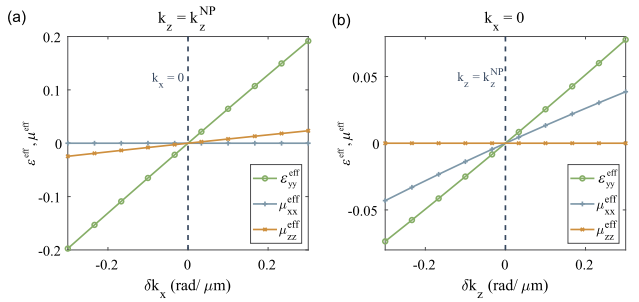

Fig. 2. Effective parameters varying with (a) δk_x and (b) δk_z, calculated by matching the dispersion and impedance. $\varepsilon_{yy}^{\text{eff}}$, μ_{xx}^{eff}, and μ_{zz}^{eff} all tend to zeros in the reciprocal space with $\mathbf{k}^{NP\pm} = \left(0, 0, k_z^{NP}\right)$.

with the velocity $-\mathbf{v} = -c^2\mathbf{k}^{\text{NP}_\pm}/\omega^{\text{NP}}$ relative to the laboratory reference. Inversely, the stacked PhC at the NPs can be deemed as an effective MDZIM traveling with speed $\mathbf{v}$ along the z axis, which gives rise to an effective antisymmetric magnetoelectric coupling term [χ in Eq. (2)]:

$$\chi = \left(1 - n^2\right)\begin{pmatrix} 0 & v/c & 0 \\ -v/c & 0 & 0 \\ 0 & 0 & 0 \end{pmatrix}. \tag{3}$$

Based on the nonlocal effective medium approach [27], we can retrieve the components of $\bar{\varepsilon}^{\text{eff}}$, $\bar{\mu}^{\text{eff}}$ around the NPs for odd modes $\psi_1 = (E_y, H_x, H_z)^\intercal$ propagating in the $k_y = 0$ plane (see Supplement 1 S2):

$$\varepsilon_{yy}^{\text{eff}} = \frac{1}{\omega^2}\left[k_x\left(k_x + \frac{2\pi}{L}\right) + k_z^2\left(1 - \frac{\omega\, k_z^{\text{NP}_\pm}}{\omega^{\text{NP}} k_z}\right)\right],$$
$$\mu_{xx}^{\text{eff}} = 1 - \frac{\omega\, k_z^{\text{NP}_\pm}}{\omega^{\text{NP}} k_z}, \quad \mu_{zz}^{\text{eff}} = \frac{k_x}{k_x + \frac{2\pi}{L}}.$$

At the NPs, except for the antisymmetric magnetoelectric coupling arising from the effective velocity, all the constitutive parameters are reduced to zero $\varepsilon_{yy}^{\text{eff}} = \mu_{xx}^{\text{eff}} = \mu_{zz}^{\text{eff}} = 0$; thus, the PhC at NPs is equivalent to a MDZIM, as shown in Fig. 2.

According to the effective medium theory, a spin-1 Dirac-like cone at Γ results in effective zero permittivity and permeability, denoted as DZIM. However, the MDZIM discussed here represents a DZIM moving at a constant velocity in the z direction. This configuration of an ideal MDZIM could enable a similar tunneling and cloaking phenomenon at a specific incident angle compared with the DZIM. As shown in Fig. 3(a), Maxwell's equations for the TE incidence ($E_z = 0$) in region A_1 read as follows:

$$\nabla \times \mathbf{H} = -i\omega\mathbf{D} = -i\omega\left(\varepsilon_{A_1}\mathbf{E} - \left(1 - n^2\right)\frac{\mathbf{v}}{c^2} \times \mathbf{H}\right),$$

where $\varepsilon_{A_1} = 0$. The continuous translational symmetry along the z direction gives $\nabla\times \to \nabla_{xy} \times + ik_z\hat{\mathbf{z}}\times$. When $k_z\hat{\mathbf{z}} = \omega\left(1 - n^2\right)\mathbf{v}/c^2$, we have the following:

$$\nabla_{xy} \times \mathbf{H} = 0 \Rightarrow \partial_{\mathbf{x}}\mathbf{H}_z = \partial_{\mathbf{y}}\mathbf{H}_z = 0. \tag{4}$$

Therefore, $H_z^{A_1} = const.$ is always established in the region of MDZIMs for TE waves. Hence, at the input and output interfaces (b_1 and b_2), the out-of-plane component of magnetic fields satisfies $H_z^{in}(1 + R) = H_z|_{b_1} = H_z^{A_1} = H_z|_{b_2} = H_z^{in}T$, which leads

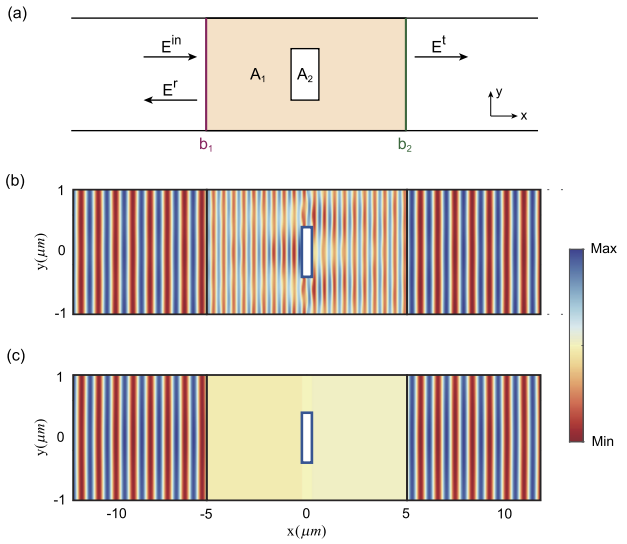

Fig. 3. (a) Sketch of angle-dependent perfect tunneling in the MDZIM for TE incident waves. Simulation of a plane wave ($\hat{M}_y$-odd modes) obliquely impinging upon (b) layer-stacked PhC and an (c) ideal MDZIM. The blue rectangle surrounded by the PhC (MDZIM) is a PEC barrier with a width of 0.5 μm and a height of 1 μm. In both cases, the background medium of two sides ($|x|$ >5μm) is a static dielectric with relative permittivity $\varepsilon = 2.2$. The PhC has the same parameters with the one in Fig. 1. The MDZIM has parameters $\varepsilon^{\text{eff}} = \mu^{\text{eff}} = 0$ and $\mathbf{v} = c^2\mathbf{k}^{NP_+}/\omega^{NP}$. Periodic boundary conditions are applied to the upper and lower boundaries. The plane wave is incident from the left side with the incident wave vector $\mathbf{k}^{in} = \left(k_x^{in}, 0, k_z^{NP_+}\right)$ and wavelength $\lambda = 2\pi c/\omega^{NP} = 1.427\mu$m.

to $T = 1 + R$. Consider Faraday's law in region A_1:

$$\oint_{\partial A_1} \mathbf{E} \cdot d\mathbf{l} = -i\omega \int_{A_1} \mu_{A_1} H_z dS = 0, \tag{5}$$

where $\mu_{A_1} = 0$ has been used. We have the following:

$$\oint_{\partial_{A_1}} \mathbf{E} \cdot d\mathbf{l} = \int_{b_2 - b_1} \mathbf{E} \cdot d\mathbf{l} - \oint_{\partial_{A_2}} \mathbf{E} \cdot d\mathbf{l}, \tag{6}$$

where $\oint_{\partial_{A_2}} \mathbf{E} \cdot d\mathbf{l} = 0$ because the electric fields only have only normal component of the PEC inclusions (A_2). Thus, Eq. (6) reduces into the following:

$$\oint_{\partial_{A_1}} \mathbf{E} \cdot d\mathbf{l} = \left(E_y^t + E_y^r - E_y^{in}\right) d$$
$$= (T + R - 1)\, H_z^{in} Z_x d = 2RH_z^{in} Z_x d, \tag{7}$$

where d is the height of region A_1 and Z_x is the impedance at the input and output boundaries. Equations (5) and (7) lead to $R = 0$. Therefore, the MDZIM slab does support angle-dependent perfect tunneling (at the specific out-of-plane wavenumber $k_z = v/c^2$) for arbitrary PEC inclusions, with the conditions that the moving direction is parallel to the slab boundaries and the incident electric field is normal to the moving direction.

In order to demonstrate that the PhC here indeed behaves as a MDZIM, we simulated the tunneling effect for a plane wave obliquely impinging from a static background dielectric medium upon the $x = const.$ plane of the layer-stacked PhC and of an ideal MDZIM with the velocity $\mathbf{v} = c^2\mathbf{k}^{NP_+}/\omega^{NP}$ respectively, where

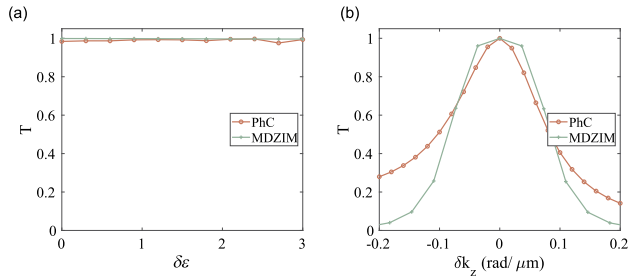

Fig. 4. Transmittance (T) varies with the (a) relative permittivity ε of the background medium and with (b) $\delta k_z = k_z^{in} - k_z^{NP+}$ (difference between the k_z component of the incident wave and k_z^{NP+}).

a rectangular PEC barrier embeds in both structures. The angular frequency of the incident wave is fixed at $\omega^{\text{in}=\omega^{NP}}$, and the incident wave vector $\mathbf{k}_{\text{in}}$ lies in the $k_y = 0$ plane. The incident plane wave has an odd mirror parity (only the electric field has a component in the y direction). When the k_z component of $\mathbf{k}^{\text{in}}$ equals k_z^{NP+}, the refractive wave inside the PhC hits the NP at $\mathbf{k}^{NP+}$ in the momentum space, and the simulation result in Fig. 3(b) demonstrates that the wave can pass through the PhC without backscattering and phase retardation along the x direction, and thus the PEC obstacle is cloaked. The moving DZIM after transformation still has zero permittivity and permeability, but has a nonzero magnetoelectric coupling coefficient. Figure 3(c) demonstrates that the ideal MDZIM produces exactly the same cloaking effect, thereby confirming the equivalence between the effective MDZIM and the PhC at the NP.

Furthermore, Fig. 4(a) shows that the transmittance remains at nearly 100% when changing the dielectric constant of the background medium in both cases, demonstrating that the MDZIM inherits the exotic property of universal impedance matching with an arbitrary background medium featured by the ordinary DZIM (see more discussions in Supplement 1 S3). However, altering the oblique angle of the incident wave significantly reduces the transmittance when the k_z^{in} component deviates from k_z^{NP+}, as depicted in Fig. 4(b). This indicates a high sensitivity of the effect to the incident angle. Additionally, the divergence between the two curves in Fig. 4(b) arises because the effective medium of the photonic crystal (PhC) diverges from that of a moving double-zero-index medium (MDZIM) when $k_z \neq k_z^{\text{NP}+}$.

In conclusion, we have uncovered the hidden symmetry-induced effective MDZIM in layer-stacked PhCs. The effective parameters of the PhC are retrieved using the nonlocal effective medium approach, which shows that both the effective permittivity and permeability tend toward zero around NPs, while an antisymmetric magnetoelectric coupling persists, mimicking the effect of a moving medium. Perfect tunneling and universal impedance matching effects are demonstrated for both PhC and ideal MDZIM configurations. Furthermore, an angle-dependent transmittance phenomenon emerges when the incident angle is altered, consistent with predictions from the effective medium theory. Unlike the 2D DZIM approach, which relies on a fully accidental triple degeneracy, the symmetry-enforced nature of the triple NPs ensures that the effective MDZIM can be realized in almost all PhCs that respect the corresponding symmetries.

For applications, the effective moving velocity of the MDZIM can be freely adjusted by tuning the locations of the NPs away from Γ. When the NPs are shifted to the region under the light line of the background medium, waves propagating in MDZIM slabs with finite thickness in the y direction can avoid out-of-plane radiation. The angle-dependent perfect tunneling also breaks the paradigm of the normal incidence condition of the DZIM. This opens the door to applications of zero-index materials, including large area and ultra-low loss wavefront engineering and angle-dependent beam filters. The implements of this PhC with a liquid crystal or effective anisotropic medium exhibit the possibilities of flexible incident angle and on-chip applications.

Funding. Croucher Foundation (CAS20SC01); The Innovation Project of Optics Valley Laboratory; National Natural Science Foundation of China (12274161).

Disclosures. The authors declare no conflicts of interest.

Data availability. Data underlying the results presented in this paper may be obtained from the authors upon reasonable request.

Supplemental document. See Supplement 1 for supporting content.

REFERENCES

1. L. Lu, L. Fu, J. D. Joannopoulos, *et al.*, Nat. Photonics **7**, 294 (2013).
2. W.-J. Chen, M. Xiao, and C. T. Chan, Nat. Commun. **7**, 13038 (2016).
3. J. Noh, S. Huang, D. Leykam, *et al.*, Nat. Phys. **13**, 611 (2017).
4. Q. Guo, O. You, B. Yang, *et al.*, Phys. Rev. Lett. **122**, 203903 (2019).
5. B. Bradlyn, J. Cano, Z. Wang, *et al.*, Science **353**, aaf5037 (2016).
6. L. Lu, C. Fang, L. Fu, *et al.*, Nat. Phys. **12**, 337 (2016).
7. H. Watanabe and L. Lu, Phys. Rev. Lett. **121**, 263903 (2018).
8. Z. Xiong, R.-Y. Zhang, R. Yu, *et al.*, Light: Sci. Appl. **9**, 176 (2020).
9. X. Huang, Y. Lai, Z. H. Hang, *et al.*, Nat. Mater. **10**, 582 (2011).
10. N. I. Zheludev and Y. S. Kivshar, Nat. Mater. **11**, 917 (2012).
11. H. Chu, Q. Li, B. Liu, *et al.*, Light: Sci. Appl. **7**, 50 (2018).
12. Y. Yang, Y. Liu, J. Qin, *et al.*, Photonics Res. **11**, 1613 (2023).
13. A. Alu, M. G. Silveirinha, A. Salandrino, *et al.*, Phys. Rev. B **75**, 155410 (2007).
14. Y. Jing, J. Xu, and N. X. Fang, Phys. Lett. A **376**, 2834 (2012).
15. R. Fleury and A. Alù, Phys. Rev. Lett. **111**, 055501 (2013).
16. M. Silveirinha and N. Engheta, Phys. Rev. Lett. **97**, 157403 (2006).
17. B. Edwards, A. Alù, M. E. Young, *et al.*, Phys. Rev. Lett. **100**, 033903 (2008).
18. I. Liberal and N. Engheta, Nat. Photonics **11**, 149 (2017).
19. R. W. Ziolkowski, Phys. Rev. E **70**, 046608 (2004).
20. V. C. Nguyen, L. Chen, and K. Halterman, Phys. Rev. Lett. **105**, 233908 (2010).
21. Y. Wu and J. Li, Appl. Phys. Lett. **102**, 183105 (2013).
22. J. Hao, W. Yan, and M. Qiu, Appl. Phys. Lett. **96**, 101109 (2010).
23. A. M. Mahmoud and N. Engheta, Nat. Commun. **5**, 5638 (2014).
24. C. Xu, K. Lyu, and Y. Wu, Europhys. Lett. **141**, 15002 (2023).
25. D. H. Staelin, A. W. Morgenthaler, and J. A. Kong, *Electromagnetic Waves* (Pearson Education India, 1994).
26. P. Moitra, Y. Yang, Z. Anderson, *et al.*, Nat. Photonics **7**, 791 (2013).
27. J. Luo, Y. Yang, Z. Yao, *et al.*, Phys. Rev. Lett. **117**, 223901 (2016).